ENVIRONMENTAL STUDIES

How close are we to the temperature tipping point of the terrestrial biosphere?

Katharyn A. Duffy[1,2]*, Christopher R. Schwalm[2,3], Vickery L. Arcus[4], George W. Koch[2], Liyin L. Liang[4,5], Louis A. Schipper[4]

The temperature dependence of global photosynthesis and respiration determine land carbon sink strength. While the land sink currently mitigates ~30% of anthropogenic carbon emissions, it is unclear whether this ecosystem service will persist and, more specifically, what hard temperature limits, if any, regulate carbon uptake. Here, we use the largest continuous carbon flux monitoring network to construct the first observationally derived temperature response curves for global land carbon uptake. We show that the mean temperature of the warmest quarter (3-month period) passed the thermal maximum for photosynthesis during the past decade. At higher temperatures, respiration rates continue to rise in contrast to sharply declining rates of photosynthesis. Under business-as-usual emissions, this divergence elicits a near halving of the land sink strength by as early as 2040.

INTRODUCTION

The difference between gross primary productivity, carbon uptake by vegetation, and total ecosystem respiration, carbon loss to the atmosphere, comprises the metabolic component of the land carbon sink [net ecosystem productivity (NEP)]. To date, land ecosystems provide a climate regulation service by absorbing ~30% of anthropogenic emissions annually [mean ± 1 SD: 2.6 petagrams carbon (PgC) ± 0.8 $year^{-1}$] (*1*). While temperature functions as a key driver of year-to-year changes in the land carbon sink (*2*), its temperature response is still poorly constrained at biome to global scales (*3*, *4*), making the carbon consequences of anticipated warming uncertain.

Like all biological processes, metabolic rates for photosynthesis and respiration are temperature dependent; they accelerate with increasing temperature, reach a maximum rate, and decline thereafter. Yet, these carbon fluxes do not necessarily have the same temperature response, potentially resulting in sharp divergences in ecosystem carbon balance. For example, increasing respiration rates without corresponding increases in photosynthesis rates would decrease the efficacy of the terrestrial carbon sink. An observational constraint on the net difference in metabolic response across both gross fluxes is thus urgently needed to constrain projections of the future land carbon sink and, more specifically, isolate points of nonlinear and perhaps nonreversible change—tipping points (*5*). This is especially relevant given the highly divergent land carbon sink trajectories from Earth system models (*4*) that, nevertheless, agree on continued future increases in sink strength due to the CO_2 fertilization effect (*3*).

Given in situ evidence that regions of the terrestrial biosphere are experiencing temperature thresholds at which they switch from a carbon sink to source (*6*–*8*), we asked the following questions: (i) What are the thermal maxima of photosynthesis (T_P^{max}) and respiration (T_R^{max}) at biome to global scales? (ii) What is the thermal maximum for the land sink of carbon (T_{NEP}^{max}) and current mean temperature range with regard to this critical threshold? (iii) At what global and regional temperatures do we expect the land sink of carbon to decline? (iv) Are those temperatures in the foreseeable future?

To address these questions, we used measurements from the largest continuous carbon monitoring network, FLUXNET (*9*), as an observational constraint to determine the temperature dependence of global rates of photosynthesis and respiration. Across ~1500 site years of daily data from all major biomes and plant functional types, we applied a 30-day moving window partial correlation analysis at each flux tower site to extract the temperature signal (a change in photosynthesis or respiration solely attributable to changes in temperature, i.e., the signal excludes other climatic effects such as water availability and sunlight) from daytime partitioned gross primary productivity [photosynthesis (P)] and total ecosystem respiration (R). We then normalized each site-level temperature dependence curve and applied macromolecular rate theory (MMRT) (*10*) in conjunction with Monte Carlo resampling to avoid length-of-record bias. The curves were subsequently aggregated to the biome level and then area-weighted to arrive at a global constraint of temperature dependence (see Materials and Methods). MMRT is a framework rooted in the principles of thermodynamics, which provides a mechanistic basis to extract the temperature dependence of rates across scales from individual enzyme kinetics to organismal and ecosystem metabolism (see Materials and Methods) (*11*). This framework is based on classical transition state theory from physical chemistry (*12*) and describes temperature rate dependence using three parameters, with emphasis on a maximum or optimal temperature value, T^{max}, above which rates decline exponentially. The Arrhenius function is a special case of MMRT where the heat capacity term is zero and the temperature-rate relationship is exponential without a maximum (see Materials and Methods) (*10*). MMRT is applicable across a range of processes and levels of biological organization and has been successfully used to model the temperature dependence of enzyme kinetics (*13*), microbial growth (*14*), soil respiration (*15*), and leaf respiration (*16*). Here, we extend this analysis to include global land photosynthesis and net carbon fluxes, producing the first observationally derived curves for the temperature dependence of global carbon metabolism, using a single function grounded in thermodynamics.

[1]School of Informatics, Computing and Cyber Systems, Northern Arizona University, Flagstaff, AZ 86011, USA. [2]Center for Ecosystem Science and Society, Northern Arizona University, Flagstaff, AZ 86011, USA. [3]Woods Hole Research Center, Falmouth, MA 02540, USA. [4]School of Science, University of Waikato, Hamilton 3216, New Zealand. [5]Manaaki Whenua–Landcare Research, Private Bag 11052, Palmerston North 4442, New Zealand.
*Corresponding author. Email: katharyn.duffy@nau.edu

Definitions:

Temperature signal: A change in photosynthesis or respiration solely attributable to changes in temperature, i.e., the signal excludes other climatic effects such as water availability and sunlight.

Tipping point: This denotes the temperature threshold at which the global land surface will switch from a carbon sink to a carbon source when—due solely to temperature—photosynthesis is in exponential decline while respiration is in exponential increase.

Thermal maxima: The thermal maximum (T^{max}) represents the peak of the temperature dependence curve where any additional increase in temperature will decrease the metabolic rate of either photosynthesis or respiration.

Warmest Quarter: Mean temperature of warmest quarter (3-month period)

RESULTS

In FLUXNET, the temperature response of global photosynthesis shows distinct maxima (T_P^{max}) at 18° and 28°C for C_3 and C_4 plant systems, respectively (Fig. 1). While the maximum for C_3 plants is lower than optima observed in leaf-level measurements (*17*, *18*), our estimates validate lower T_P^{max} estimates derived elsewhere at the ecosystem scale (*19*). Furthermore, our estimates are based on ambient temperature and total ecosystem CO_2 exchange and so are more directly relevant to global predictions for warming, which track global mean surface temperature as opposed to leaf temperature. In general, leaf temperatures are both (i) highly variable at even the individual plant level and (ii) poorly constrained at Earth system scales, making ambient air temperature a more suitable metric for investigating future response. Moreover, the maximum that we report is derived from observations that are restricted to temperatures experienced by ecosystems rather than the broader range imposed in controlled environment studies.

In contrast to photosynthesis, respiration rates increase across the range of ambient temperatures observed by FLUXNET (up to 38°C) (*9*), with no evidence of T_R^{max} or rate decline. Using MMRT on experimental manipulations of leaf and soil respiration—together, ~87% of total ecosystem respiration (*20*, *21*)—demonstrates that the thermal maxima of leaf and soil respiration T_R^{max} reside at ~60° and 70°C, respectively (*15*, *16*). This is far above temperatures observed at tower sites (*9*) and any near-term projections under any warming scenario (*22*). The high thermal maxima of leaf and soil respiration from experimental data are in agreement with the exponential increase in rate observed within ambient temperature FLUXNET data (fig. S1 and see Materials and Methods) and far above those for C_3 and C_4 photosynthesis. Temperatures where photosynthesis begins to decline are concurrent with the steepest increase in respiration rates for all datasets considered (*9*, *15*, *16*). Small changes in temperature past this point show opposite trends in the rates of photosynthesis and respiration. The large disparity between T^{max} values for photosynthesis and respiration (autotrophic and heterotrophic combined) implies that flux responses diverge at temperatures above T_P^{max} and that the imbalance grows more pronounced as temperature increases.

With temperature dependencies of both gross fluxes, we use mass balance to derive the optimal temperature of net land carbon uptake (T_{NEP}^{max}) and find that, currently, the mean temperature of the warmest quarter (3-month period) extends just past T_{NEP}^{max} (blue curve, Fig. 2). Our observationally derived temperature dependence curves explain both the current substantial sink of the biosphere (*23*, *24*) and documented episodes of rapid release of carbon to the atmosphere during high temperature extremes (*6*–*8*). Current climate mostly lies just below T_{NEP}^{max}, i.e., where slight increases in temperature act as climate fertilization of land carbon uptake. Under anticipated warming—as foreshadowed by historical temperature extremes and coincident land carbon loss—however, more and more time will be spent above T_{NEP}^{max}. Past this threshold, the land carbon balance will first weaken and ultimately reverse sign from carbon sink to carbon source.

This link between anticipated warming and declines in land carbon uptake is a function of differential responses of gross fluxes to temperature. At temperatures up to the inflection point for photosynthesis, respiration and photosynthesis are effectively "coupled"—both processes increase with increasing temperature, albeit at different rates. At temperatures above the inflection point for photosynthesis, however, these processes become increasingly "decoupled." That is, the rate of increase slows for photosynthesis and, past T_P^{max}, declines exponentially. Throughout this temperature range, respiration continues to increase exponentially. This decoupling acts to severely degrade the land carbon sink. It is important to note that the extension of the warmest quarter past T_{NEP}^{max} at FLUXNET sites is largely a recent phenomenon. When separated across greater than two decades of FLUXNET observations, the mean temperature of the warmest quarter has increased by 1.8°C, pushing current climate space past global T_P^{max} and thus into a regime of declining photosynthetic rates (see Materials and Methods). Given that the mean temperature of the warmest quarter currently extends just past estimates of T_{NEP}^{max}, any additional warming will both move mean climate past the inflection point for photosynthesis, effectively slowing land carbon uptake, and increase the cumulative amount of time past T_P^{max}, where photosynthesis is negatively affected. Simultaneously, the response of respiration would be nearly exponential (*9*, *14*–*16*). This intersection (25°C) constitutes a powerful tipping point for the land sink of carbon and a formidable positive climatic feedback (Fig. 2).

Currently, less than 10% of the terrestrial biosphere experiences temperatures past T_P^{max}, where land carbon uptake is degraded (Fig. 3A). For regions that do experience these temperatures, exposure is limited to 1 to 2 months or constitutes areas with sparse to no vegetation. Under business-as-usual emissions, by 2100, up to half of the terrestrial biosphere could experience temperatures past T_P^{max}, a three- to fivefold increase, based on uncertainty in temperature projections, over current levels (Fig. 3, B and C). However, the impact of elevated temperatures on the land sink is more than a function of cumulative area. Biomes that cycle 40 to 70% of all terrestrial carbon (*19*) including the rainforests of the Amazon and Southeast Asia and the Taiga forests of Russia and Canada are some of the first to exceed biome-specific T_P^{max} for half the year or more. This reduction in land sink strength is effectively front-loaded in that a 45% loss occurs by midcentury, with only an additional 5% loss by the end of the century (Fig. 3D). Furthermore, these estimates are conservative as they assume full recovery of vegetation after temperature stress and ignore patterns and lags in recovery (*25*).

DISCUSSION

Our findings demonstrate temperature limits for global photosynthesis rates and the terrestrial land sink as a whole. Despite two

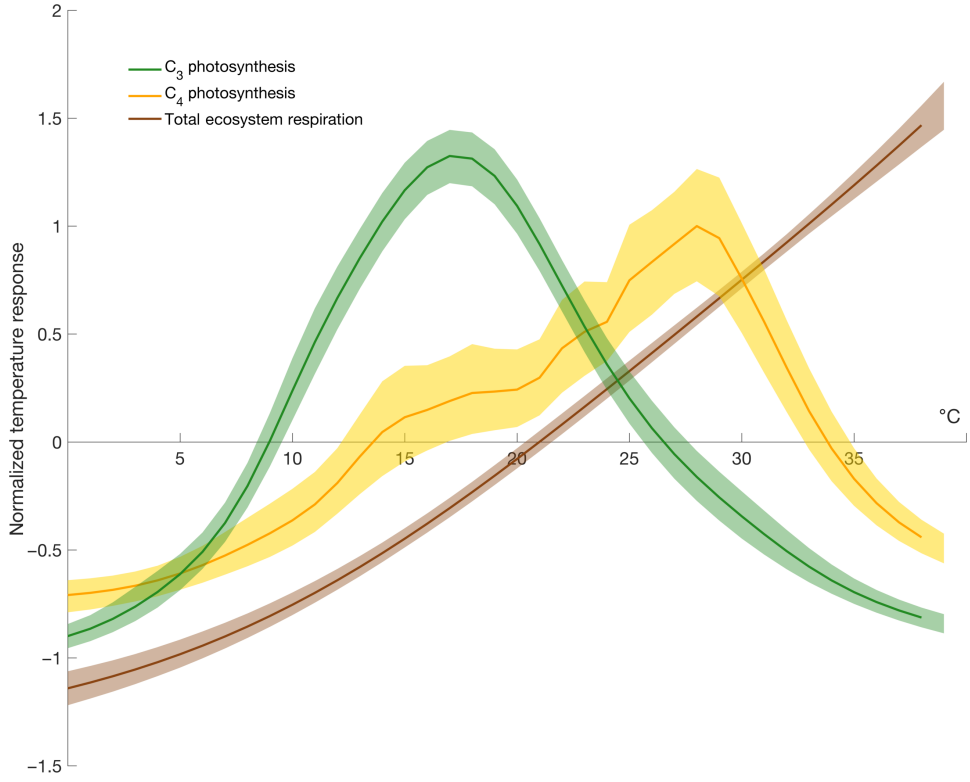

Fig. 1. Temperature dependence of global carbon fluxes. The normalized global temperature response of C_3 photosynthesis (green), which exhibits T_P^{max} of 18°C, C_4 photosynthesis (yellow) that exhibits T_P^{max} at 28°C, and total ecosystem respiration (brown) derived from the FLUXNET 2015 synthesis dataset. The minor thermal optima observed in C_4 classified sites validate the mixed C_3/C_4 nature of some ecosystems and were well explained by the sum of two Gaussian curves (see Materials and Methods). All fluxes were normalized and fit over ambient temperatures observed by FLUXNET (up to 38°C), where the mean across each curve sums to zero. Shaded areas represent the 90% confidence interval of projections.

decades of FLUXNET observations and the warmest decade on record, we observed no evidence of acclimation in photosynthesis (see Materials and Methods and fig. S2). While it is possible that temperature adaptation could mitigate the size of this impact, given high daily, seasonal, and interannual variation in temperature, as opposed to uniform warming from experimental data, the likelihood of detecting acclimation is low. Furthermore, two decades is likely too short a period to see selection for genotypes with higher temperature tolerance, particularly in systems dominated by perennial plants (*16*–*28*). Given current proximity to T_P^{max} with no acclimation observed, it is unlikely that acclimation will proceed with sufficient speed to compensate for temperature-induced declines (*29*).

Beyond acclimation, and despite an increase of ~40-ppm_v (parts per million by volume) CO_2 over the 1991–2015 FLUXNET record, we also observed no notable alteration in the magnitude of photosynthesis across the data record (fig. S3). We note that, on the basis of the solubility of CO_2 as a function of temperature and pressure, leaf water affinity for CO_2 is nearly unchanged across the data record (*30*). We therefore contend that, in contrast to any CO_2 fertilization effect (*3*), anticipated higher temperatures associated with elevated CO_2 could degrade land carbon uptake and that failure to account for this results in a gross overestimation of climate change mitigation provided by terrestrial vegetation. We note that future work accounting for the timing of photosynthetic activity (*31*), CO_2 concentrations, and the solubility of CO_2 as a function of temperature (*30*) will be essential to accurately predict the role of CO_2 fertilization in the land sink of carbon (*32*).

The temperature tipping point of the terrestrial biosphere lies not at the end of the century or beyond, but within the next 20 to 30 years (Figs. 2 and 3, A to D). Given the temperature limits of land carbon uptake presented here, without mitigating warming, we will cross the temperature threshold of the most productive biomes by midcentury, after which the land sink will degrade to only ~50% of current capacity if adaptation does not occur. While biomes will eventually shift spatially in response to warming, this process is unlikely to be a smooth migration, but rather a rapid disturbance-driven loss of present biomes (with additional emissions of carbon to the atmosphere), followed by a slower establishment of biomes more suited to the emerging climate. Furthermore, the establishment of new biomes is unlikely to be complete without human intervention and will be limited by edaphic factors, especially nutrient availability. This further suggests that we are rapidly entering temperature regimes where biosphere productivity will precipitously decline and calls into question the future viability of the land sink, along with Intended Nationally Determined Contributions (INDCs) within the Paris Climate Accord, as these rely heavily on land uptake of carbon to meet pledges (*33*). In contrast to Representative Concentration Pathway 8.5 (RCP8.5), warming associated with scenario RCP2.6 could allow for near-current levels of biosphere productivity, preserving the majority land carbon uptake (~10 to 30% loss). Failure to implement agreements that meet or exceed limits in the Paris Accord could quantitatively alter the large and persistent terrestrial carbon sink, on which we currently depend to mitigate anthropogenic emissions of CO_2 and therefore global environmental change.

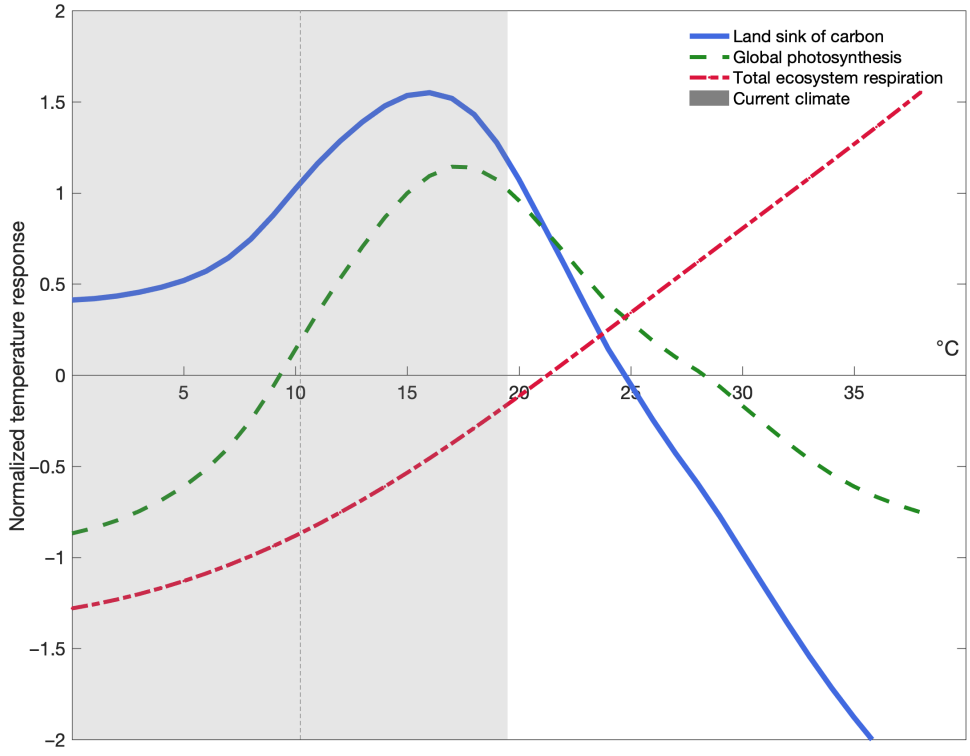

Fig. 2. Temperature dependence of the terrestrial carbon sink. Integrated global temperature response curves for normalized photosynthesis (green dashed line), respiration (red dashed dotted line), and a mass balance estimate of the land sink (blue solid line) in relation to current climate (gray bar), where the mean across each curve sums to zero. Photosynthesis represents the integration of C_3 and C_4 curves (Fig. 1) weighted by global fraction of C_3/C_4 photosynthesis (*37*). The gray shaded bar represents observed mean annual temperature range from 1991 to 2015 (*9*, *22*), and vertical dashed line indicates current annual mean temperature at FLUXNET tower sites.

MATERIALS AND METHODS

Macromolecular rate theory

MMRT is based on classic transition state theory that describes the temperature dependence of chemical reaction kinetics using statistical thermodynamics (*6*). A central tenant of MMRT is the explicit recognition of the change in heat capacity for enzyme-catalyzed rates, $\Delta C_P^{\ddagger}$—the difference in heat capacity between the enzyme-substrate (ES) complex and the enzyme–transition state (E-TS) complex. The heat capacity for large macromolecules such as enzymes is a function of the distribution of vibrational modes for the system.

For MMRT, the heat capacity term is incorporated into the Eyring equation to give Eq. 1 below. The resultant signature of MMRT is a curved plot of rate versus temperature in the absence of denaturation. $\Delta C_P^{\ddagger}$ determines the curvature of such a plot, and an important component of $\Delta C_P^{\ddagger}$ is the change in the distribution of vibrational modes in each state along the reaction coordinate (ES and E-TS complexes) (*34*)

$$k = \frac{k_B T \kappa}{h} e^{\frac{-\Delta G^{\ddagger}}{RT}} = \frac{k_B T \kappa}{h} e^{\left[\frac{-\Delta H^{\ddagger}_{T_0} - \Delta C^{\ddagger}_P (T - T_0)}{RT} + \frac{\Delta S^{\ddagger}_{T_0} + \Delta C^{\ddagger}_P (\ln T - \ln T_0)}{R}\right]} \quad (1)$$

Equation 1 (based on transition state theory) lies at the heart of MMRT. It describes the rate (k) in terms of the Boltzmann, Planck, and universal gas constants (k_B, h, and R, respectively), absolute temperature (T), the transmission coefficient (κ), the change in enthalpy ($\Delta H^{\ddagger}_{T_0}$) and entropy ($\Delta S^{\ddagger}_{T_0}$) between ground and transition states at a reference temperature (T_0), and the change in heat capacity between ES and E-TS complexes ($\Delta C_P^{\ddagger}$). Thus, the first derivative of MMRT quantifies the change in rate (k) relative to change in temperature (T), given in Eq. 2

$$\frac{dk}{dT} = k\left(\frac{1}{T} + \frac{\Delta H^{\ddagger}_{T_0} + \Delta C^{\ddagger}_P (T - T_0)}{R T^2}\right) \quad (2)$$

We have previously demonstrated that MMRT accurately describes the temperature dependence of biological rates at increasing levels of complexity [microbial growth rates (*14*), soil respiration (*15*), and plant respiration (*16*)]. This provides justification for using MMRT in for analysis of the temperature dependence of ecosystem fluxes in the FLUXNET dataset.

FLUXNET data and processing

As an observational dataset for the temperature dependence of land carbon fluxes, mean daily estimates of carbon fluxes and micrometeorological variables were retrieved from the FLUXNET 2015 synthesis dataset for all tier 1 and tier 2 sites, along with uncertainty estimates based on gap filling and SD of fluxes (*35*). The daytime partitioning algorithm was selected for estimates of gross primary productivity (P) and total ecosystem respiration (R) to minimize bias associated with constraining the temperature response of partitioned fluxes through nighttime temperatures (*36*). Concurrent estimates of air temperature, latent and sensible heat, and downwelling shortwave radiation flux were also extracted, along with metrics for gap-filling of flux and meteorological data.

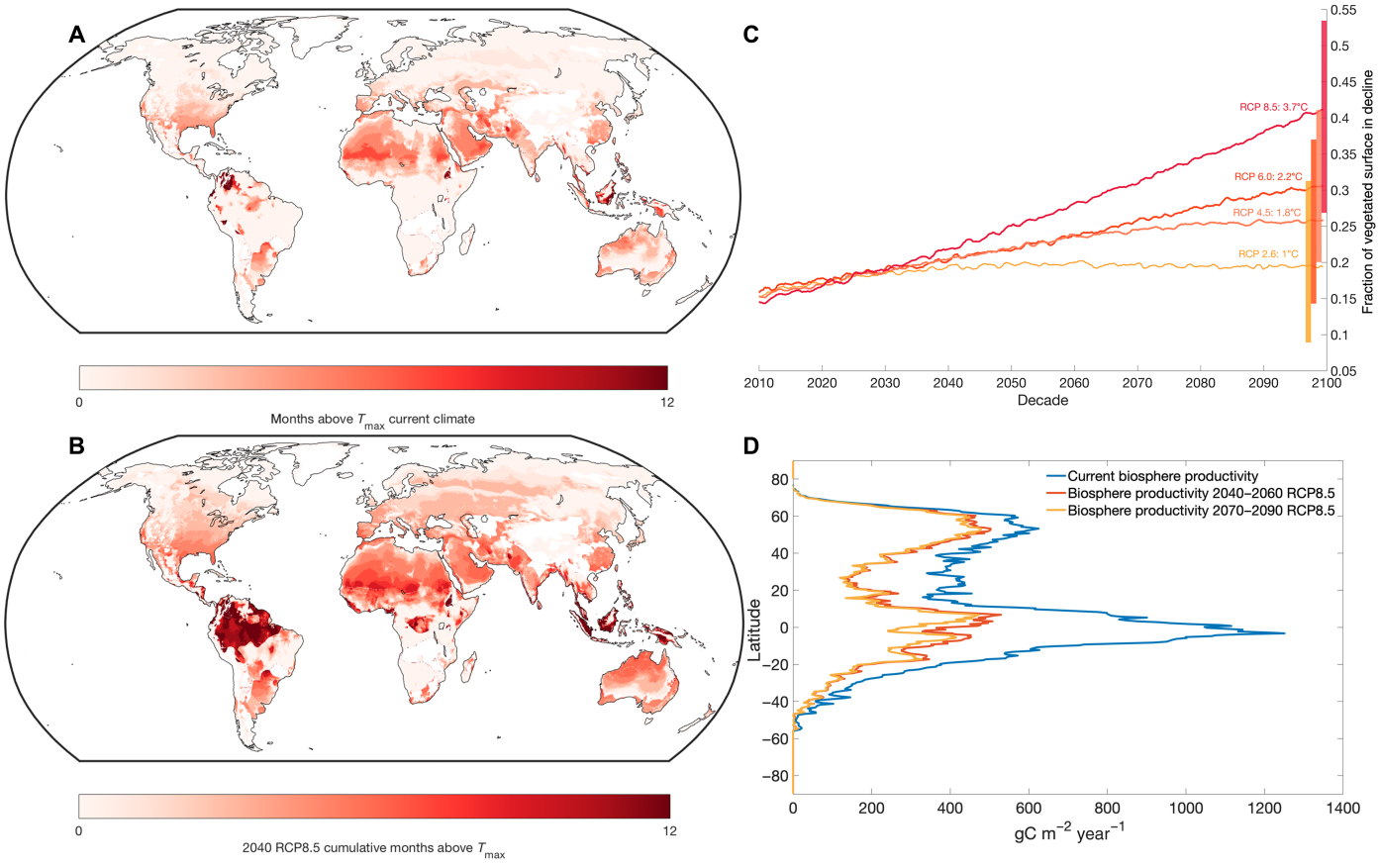

Fig. 3. Spatial patterns of temperature tipping points for the biosphere. (**A**) Current cumulative monthly dose of temperature above T_P^{max} by biome (see Materials and Methods) based on 1950–2010 WorldClim data (*22*). (**B**) Cumulative temperature dose above T_P^{max} under Representative Concentration Pathway 8.5 (RCP8.5) by 2040–2060 based on WorldClim data (*22*). (**C**) Cumulative fraction of terrestrial biosphere in exceedance of T_P^{max} by RCP scenario based on Coupled Model Intercomparison Project Phase 5 (CMIP5) multimodel mean monthly data. Vertical bars represent an integration of the uncertainty across CMIP5 ensemble member projections for changes in temperature, translated into a range of exceedance of T_P^{max} for the vegetated surface. (**D**) Current mean gridded gross photosynthesis (2003–2013) (*38*) along with reductions in biosphere productivity due to exceedance of T^{max} for 2040–2060 (44% reduction) and 2070–2090 (49% reduction) based on Worldclim CMIP5 downscaled data (*22*).

Combined, latent and sensible heat were used to calculate evaporative fraction (EF), the inverse of the Bowen ratio, and a robust index of relative water availability to the biosphere (Eq. 3) (*37*)

$$\mathrm{EF} = \frac{\lambda E}{\lambda E + H} \quad (3)$$

where λE represents latent heat (watts per square meter) and H represents sensible heat (watts per square meter).

EF is an effective metric to assess water availability as it captures the signal from a multitude of potential water pools (e.g., soil moisture and precipitation) through evapotranspirative fluxes from the biosphere and scales well globally. We also evaluated the signal of vapor pressure deficit (VPD) as an alternate metric for water stress but found no statistically significant alteration of response (fig. S4). Given large variation in productivity and climate across biomes, we normalized all carbon fluxes along with micrometeorological variables within site to avoid signals based on biogeography. To maintain in situ derivation of temperature dependence, carbon flux and temperature data that were fully gap-filled were excluded from the analysis.

Temperature signal

Both photosynthesis and respiration are known to be controlled by a number of enviroclimatic variables, namely, sunlight, water, and temperature. To isolate the temperature signal, we used a 30-day moving-window partial correlation analysis on daily estimates of daytime partitioned gross primary productivity and total ecosystem respiration, with EF, downwelling short-wave radiation, and air temperature from 0° to 38°C (from biologically relevant temperatures for metabolic activity to the upper limit of the FLUXNET record) as explanatory variables at the individual site level, and filtered for significant relationships at $P < 0.1$. The result was the proportion of variation in gross fluxes that were solely attributable to each enviroclimatic variable. We then normalized and fit the temperature response of both fluxes by site to the first derivative of MMRT (*11*) to investigate changes in metabolism as a function of temperature (Eqs. 1 and 2). As MMRT was fitted at the site level and then bootstrapped, we filtered the FLUXNET synthesis dataset for towers that had $a > 10$ statistically attributed data points to ensure that data were sufficient to constrain temperature response curvature. Temperature projections from MMRT were limited to the ambient temperature window of observations from the FLUXNET record (0° to 38°C, the upper limit of FLUXNET observations).

T^{max} or tipping point determination

Two important points exist within temperature dependence curves for biosphere metabolism: the inflection point (T^{inf}) and the thermal maximum (T^{max}). The inflection point of temperature-dependent rates represents temperatures where an increase in rate (k) is maximal relative to temperature (T) and denotes where rates change from convex to concave. T_P^{inf} therefore represents the temperature at which land carbon uptake is maximal. The thermal maximum (T^{max}) represents the top of the temperature dependence curve where any additional increase in temperature will decrease metabolic rate. Here, we define T^{max} for the land sink (T_{NEP}^{max}) as the mass balance difference between T_P^{max} and T_R^{max}.

Representativeness and uncertainty of FLUXNET data

Two major challenges exist for global constraint of biosphere metabolism using the FLUXNET dataset: (i) Observations are unequally distributed across the vegetated surface, with differing lengths of record, and (ii) because of the ambient and mixed-species nature of tower observations, the data are inherently noisy. The FLUXNET dataset, however, has been shown to be statistically representative of plant functional types and Koeppen-Geiger biomes globally, suggesting that statistical analyses leveraging FLUXNET observations are robust (*38*).

To address challenges (i) and (ii), we designed a bootstrap method that sampled entire tower records rather than observations (to avoid length of record bias) to fit global curves for the temperature dependence of land carbon fluxes. We then calculated the bootstrap-to-bootstrap variation in T^{max} within Koeppen-Geiger biomes and across latitudes (fig. S2) to capture uncertainty stemming from sparse data sampling and heterogeneity of ecosystems sampled.

Bootstrapping and C_3/C_4 dichotomy

Early investigations into the temperature response of photosynthesis at global scales demonstrated a clear bimodal distribution that was well explained by C_3 and C_4 heuristics (*39*). All FLUXNET sites were therefore dichotomized into these two groups on the basis of climate criteria (*40*). The temperature response by group was then bootstrapped across the FLUXNET synthesis dataset 10,000 times, such that an entire site's temperature curve was sampled rather than specific observations, thereby decreasing the length-of-record bias and unequal distribution across bioclimatic space of some long-lived sites.

Respiration temperature signal

The exponential Arrhenius-like response of total ecosystem respiration is largely a function of ambient temperature observations, where FLUXNET effectively samples temperatures far below T_R^{max} for respiration constrained by experimental data (*15*, *16*) and largely within the inflection point for this process (fig. S1). This behavior is in full agreement with MMRT, where, for $\Delta C_P^{\ddagger}$ values close to zero, MMRT predicts Arrhenius-like behavior. To give context for the disparity in T^{max} between gross photosynthesis (P) and total ecosystem respiration (R) and to illustrate agreement between ambient temperature fitted FLUXNET data and wider-ranged experimental data, we incorporated two recent experiment-based respiration temperature response datasets (*10*, *11*), which observe T_R^{max} (fig. S1). The thermal maxima of leaf and soil respiration from these data reside at ~60° and 70°C, respectively, in alignment with ambient temperature FLUXNET predictions and far above either type of photosynthesis (fig. S1).

Evaluation of CO_2 fertilization and VPD

To evaluate the effect of CO_2 on the temperature dependence of gross primary production and the ability of CO_2 fertilization to counter temperature-induced declines in land carbon uptake, we conducted a second moving-window partial correlation analysis that included ambient CO_2 from FLUXNET towers with all other components remaining identical. While a ~1% increase in NEP per year has been correlated with elevated CO_2 elsewhere in the literature (*32*), 90% confidence intervals of the temperature dependence signal with and without CO_2 included showed no statistically significant difference (fig. S3). An identical model run was completed, replacing VPD with EF to evaluate potential changes in temperature response based on atmospheric demand rather than water flux, again demonstrating no significant differences (fig. S3).

Spatial gridding

To generate spatial grids of temperature response, FLUXNET sites were aggregated on the basis of Koeppen-Geiger climate classification regions where the FLUXNET synthesis dataset retained a coverage of >5 sites. We collapsed classes lacking sufficient replication to the next level of climatological organization. T_P^{max} was then gridded spatially on the basis of Koeppen-Geiger climate classification (fig. S4).

Cumulative dose of temperature and fraction of vegetated surface in decline

Of interest for our work was the cumulative amount of mean monthly temperatures beyond T_P^{max} within a given year. To measure this, we used FLUXNET-derived gridded T_P^{max}, WorldClim 2 at 10-min spatial resolution for current climate and WorldClim 1.4 downscaled Coupled Model Intercomparison Project Phase 5 (CMIP5) data at 10-min spatial resolution (Fig. 3, A and B) (*22*), and CMIP5 monthly data for all RCP scenarios at 2.5° resolution (Fig. 3C). We then cumulatively tallied monthly mean temperature data that exceeded T_P^{max} for both current and future climate datasets. On the basis of CMIP5 monthly data, we calculated the cumulative number of months beyond T_P^{max} and weighted them by area to assess the fraction of terrestrial land sink in decline (Fig. 3C).

Decrease in biosphere productivity RCP8.5

As biosphere productivity varies spatially, we incorporated upscaled FLUXNET data to evaluate the impacts of exceedance of T^{max} on total terrestrial biosphere productivity (*38*). To avoid biases stemming from interannual variability, we calculated mean biosphere productivity between 2003 and 2013 and evaluated temperature exceedance on the basis of our T_P^{max} grid to evaluate the number of months that each grid cell is expected to be below or above this threshold for biosphere metabolism such that pixels, which were unaffected contributed full biome productivity estimates, and biomes, which spent the entire year beyond T_P^{max}, contributed none.

Acclimation

To search for evidence of acclimation at the ecosystem-to-global scale, we first isolated FLUXNET tower sites that spanned both the first and second decades of the 2015 synthesis dataset. We then evaluated temperature dependence curves across both decades to look for upward shifts in T_P^{max} (fig. S2). Although there is evidence elsewhere in the literature supporting a shift in thermal optima at higher temperatures for individual plants, we found no evidence of this acclimation at the ecosystem-to-global scale.

Data availability

FLUXNET data access depends on the tier of data used. Tier 1 data are open and free for scientific and educational purposes, and their use follows the fair use policy accessed at https://fluxnet.fluxdata.org/data/data-policy/. Tier 2 data are from producers who are currently unable to share their data in an open manner and require an approved proposal for data access. Data access proposal information can be found at https://fluxnet.fluxdata.org/. A list of FLUXNET sites from tiers 1 and 2 used in this analysis can be found in table S3. Downscaled WorldClim CMIP5 climate data used to evaluate future climate and therefore climate space beyond T_P^{max} are freely available at http://worldclim.org/CMIP5v1. Upscaled FLUXNET data used to evaluate current and future biosphere productivity affected by temperature are freely available at www.fluxcom.org/.

SUPPLEMENTARY MATERIALS

Supplementary material for this article is available at http://advances.sciencemag.org/cgi/content/full/7/3/eaay1052/DC1

REFERENCES AND NOTES

1. T. F. Keenan, I. C. Prentice, J. G. Canadell, C. A. Williams, H. Wang, M. Raupach, G. J. Collatz, Recent pause in the growth rate of atmospheric CO_2 due to enhanced terrestrial carbon uptake. *Nat. Commun.* **7**, 13428 (2016).
2. O. Schneising, M. Reuter, M. Buchwitz, J. Heymann, H. Bovensmann, J. P. Burrows, Terrestrial carbon sink observed from space: Variation of growth rates and seasonal cycle amplitudes in response to interannual surface temperature variability. *Atmos. Chem. Phys.* **14**, 133–141 (2014).
3. D. N. Huntzinger, A. M. Michalak, C. Schwalm, P. Ciais, A. W. King, Y. Fang, K. Schaefer, Y. Wei, R. B. Cook, J. B. Fisher, D. Hayes, M. Huang, A. Ito, A. K. Jain, H. Lei, C. Lu, F. Maignan, J. Mao, N. Parazoo, S. Peng, B. Poulter, D. Ricciuto, X. Shi, H. Tian, W. Wang, N. Zeng, F. Zhao, Uncertainty in the response of terrestrial carbon sink to environmental drivers undermines carbon-climate feedback predictions. *Sci. Rep.* **7**, 4765 (2017).
4. P. Friedlingstein, M. Meinshausen, V. K. Arora, C. D. Jones, A. Anav, S. K. Liddicoat, R. Knutti, Uncertainties in CMIP5 climate projections due to carbon cycle feedbacks. *J. Climate* **27**, 511–526 (2013).
5. T. M. Lenton, H. Held, E. Kriegler, J. W. Hall, W. Lucht, S. Rahmstorf, H. J. Schellnhuber, Tipping elements in the Earth's climate system. *Proc. Natl. Acad. Sci. U.S.A.* **105**, 1786–1793 (2008).
6. P. Ciais, M. Reichstein, N. Viovy, A. Granier, J. Ogée, V. Allard, M. Aubinet, N. Buchmann, C. Bernhofer, A. Carrara, F. Chevallier, N. de Noblet, A. D. Friend, P. Friedlingstein, T. Grünwald, B. Heinesch, P. Keronen, A. Knohl, G. Krinner, D. Loustau, G. Manca, G. Matteucci, F. Miglietta, J. M. Ourcival, D. Papale, K. Pilegaard, S. Rambal, G. Seufert, J. F. Soussana, M. J. Sanz, E. D. Schulze, T. Vesala, R. Valentini, Europe-wide reduction in primary productivity caused by the heat and drought in 2003. *Nature* **437**, 529–533 (2005).
7. E. van Gorsel, S. Wolf, J. Cleverly, P. Isaac, V. Haverd, C. Ewenz, S. Arndt, J. Beringer, V. Resco de Dios, B. J. Evans, A. Griebel, L. B. Hutley, T. Keenan, N. Kljun, C. Macfarlane, W. S. Meyer, I. McHugh, E. Pendall, S. M. Prober, R. Silberstein, Carbon uptake and water use in woodlands and forests in southern Australia during an extreme heat wave event in the "Angry Summer" of 2012/2013. *Biogeosciences* **13**, 5947–5964 (2016).
8. S. Guerlet, S. Basu, A. Butz, M. Krol, P. Hahne, S. Houweling, O. P. Hasekamp, I. Aben, Reduced carbon uptake during the 2010 Northern Hemisphere summer from GOSAT. *Geophys. Res. Lett.* **40**, 2378–2383 (2013).
9. fluxdata.org, *Data Processing* (http://fluxnet.fluxdata.org//data/fluxnet2015-dataset/data-processing/), vol. 2018.
10. V. L. Arcus, E. J. Prentice, J. K. Hobbs, A. J. Mulholland, M. W. van der Kamp, C. R. Pudney, E. J. Parker, L. A. Schipper, On the temperature dependence of enzyme-catalyzed rates. *Biochemistry* **55**, 1681–1688 (2016).
11. L. A. Schipper, J. K. Hobbs, S. Rutledge, V. L. Arcus, Thermodynamic theory explains the temperature optima of soil microbial processes and high Q10 values at low temperatures. *Glob Change Biol.* **20**, 3578–3586 (2014).
12. J. K. Hobbs, W. Jiao, A. D. Easter, E. J. Parker, L. A. Schipper, V. L. Arcus, Change in heat capacity for enzyme catalysis determines temperature dependence of enzyme catalyzed rates. *ACS Chem. Biol.* **8**, 2388–2393 (2013).
13. E. J. Prentice, J. Hicks, H. Ballerstedt, L. M. Blank, L. L. Liáng, L. A. Schipper, V. L. Arcus, The inflection point hypothesis: The relationship between the temperature dependence of enzyme-catalyzed reaction rates and microbial growth rates. *Biochemistry* **59**, 3562–3569 (2020).
14. C. J. Alster, P. Baas, M. D. Wallenstein, N. G. Johnson, J. C. von Fischer, Temperature sensitivity as a microbial trait using parameters from macromolecular rate theory. *Front. Microbiol.* **7**, 1821 (2016).
15. J. M. Robinson, T. A. O'Neill, J. Ryburn, L. L. Liang, V. L. Arcus, L. A. Schipper, Rapid laboratory measurement of the temperature dependence of soil respiration and application to changes in three diverse soils through the year. *Biogeochemistry* **133**, 101–112 (2017).
16. L. L. Liang, V. L. Arcus, M. A. Heskel, O. S. O'Sullivan, L. K. Weerasinghe, D. Creek, J. J. G. Egerton, M. G. Tjoelker, O. K. Atkin, L. A. Schipper, Macromolecular rate theory (MMRT) provides a thermodynamics rationale to underpin the convergent temperature response in plant leaf respiration. *Glob. Chang. Biol.* **24**, 1538–1547 (2018).
17. S. J. Crafts-Brandner, M. E. Salvucci, Rubisco activase constrains the photosynthetic potential of leaves at high temperature and CO_2. *Proc. Natl. Acad. Sci. U.S.A.* **97**, 13430–13435 (2000).
18. G. V. Farquhar, S. von Caemmerer, J. A. Berry, A biochemical model of photosynthetic CO_2 assimilation in leaves of C_3 species. *Planta* **149**, 78–90 (1980).
19. M. Huang, S. Piao, P. Ciais, J. Peñuelas, X. Wang, T. F. Keenan, S. Peng, J. A. Berry, K. Wang, J. Mao, R. Alkama, A. Cescatti, M. Cuntz, H. de Deurwaerder, M. Gao, Y. He, Y. Liu, Y. Luo, R. B. Myneni, S. Niu, X. Shi, W. Yuan, H. Verbeeck, T. Wang, J. Wu, I. A. Janssens, Air temperature optima of vegetation productivity across global biomes. *Nat. Ecol. Evol.* **3**, 772–779 (2019).
20. M. G. Ryan, B. E. Law, Interpreting, measuring, and modeling soil respiration. *Biogeochemistry* **73**, 3–27 (2005).
21. O. K. Atkin, K. J. Bloomfield, P. B. Reich, M. G. Tjoelker, G. P. Asner, D. Bonal, G. Bönisch, M. G. Bradford, L. A. Cernusak, E. G. Cosio, D. Creek, K. Y. Crous, T. F. Domingues, J. S. Dukes, J. J. G. Egerton, J. R. Evans, G. D. Farquhar, N. M. Fyllas, P. P. G. Gauthier, E. Gloor, T. E. Gimeno, K. L. Griffin, R. Guerrieri, M. A. Heskel, C. Huntingford, F. Y. Ishida, J. Kattge, H. Lambers, M. J. Liddell, J. Lloyd, C. H. Lusk, R. E. Martin, A. P. Maksimov, T. C. Maximov, Y. Malhi, B. E. Medlyn, P. Meir, L. M. Mercado, N. Mirotchnick, D. Ng, Ü. Niinemets, O. S. O'Sullivan, O. L. Phillips, L. Poorter, P. Poot, I. C. Prentice, N. Salinas, L. M. Rowland, M. G. Ryan, S. Sitch, M. Slot, N. G. Smith, M. H. Turnbull, M. C. VanderWel, F. Valladares, E. J. Veneklaas, L. K. Weerasinghe, C. Wirth, I. J. Wright, K. R. Wythers, J. Xiang, S. Xiang, J. Zaragoza-Castells, Global variability in leaf respiration in relation to climate, plant functional types and leaf traits. *New Phytol.* **206**, 614–636 (2015).
22. R. J. Hijmans, S. E. Cameron, J. L. Parra, P. G. Jones, A. Jarvis, Very high resolution interpolated climate surfaces for global land areas. *Int. J. Climatol.* **25**, 1965–1978 (2005).
23. Y. Pan, R. A. Birdsey, J. Fang, R. Houghton, P. E. Kauppi, W. A. Kurz, O. L. Phillips, A. Shvidenko, S. L. Lewis, J. G. Canadell, P. Ciais, R. B. Jackson, S. W. Pacala, A. D. McGuire, S. Piao, A. Rautiainen, S. Sitch, D. Hayes, A large and persistent carbon sink in the world's forests. *Science* **333**, 988–993 (2011).
24. R. B. Myneni, J. Dong, C. J. Tucker, R. K. Kaufmann, P. E. Kauppi, J. Liski, L. Zhou, V. Alexeyev, M. K. Hughes, A large carbon sink in the woody biomass of Northern forests. *Proc. Natl. Acad. Sci. U.S.A.* **98**, 14784–14789 (2001).
25. C. R. Schwalm, C. A. Williams, K. Schaefer, D. Baldocchi, T. A. Black, A. H. Goldstein, B. E. Law, W. C. Oechel, R. L. Scott, Reduction in carbon uptake during turn of the century drought in western North America. *Nat. Geosci.* **5**, 551 (2012).
26. R. Bertrand, J. Lenoir, C. Piedallu, G. Riofrío-Dillon, P. de Ruffray, C. Vidal, J. C. Pierrat, J. C. Gégout, Changes in plant community composition lag behind climate warming in lowland forests. *Nature* **479**, 517–520 (2011).
27. R. T. Corlett, D. A. Westcott, Will plant movements keep up with climate change? *Trends Ecol. Evol.* **28**, 482–488 (2013).
28. K. Zhu, C. W. Woodall, J. S. Clark, Failure to migrate: Lack of tree range expansion in response to climate change. *Glob. Chang. Biol.* **18**, 1042–1052 (2012).
29. C. K. Ghalambor, J. K. McKay, S. P. Carroll, D. N. Reznick, Adaptive versus non-adaptive phenotypic plasticity and the potential for contemporary adaptation in new environments. *Funct. Ecol.* **21**, 394–407 (2007).
30. R. Weiss, Carbon dioxide in water and seawater: The solubility of a non-ideal gas. *Mar. Chem.* **2**, 203–215 (1974).
31. M. Toomey, M. A. Friedl, S. Frolking, K. Hufkens, S. Klosterman, O. Sonnentag, D. D. Baldocchi, C. J. Bernacchi, S. C. Biraud, G. Bohrer, E. Brzostek, S. P. Burns, C. Coursolle, D. Y. Hollinger, H. A. Margolis, H. McCaughey, R. K. Monson, J. W. Munger, S. Pallardy, R. P. Phillips, M. S. Torn, S. Wharton, M. Zeri, A. D. Richardson, Greenness indices from digital cameras predict the timing and seasonal dynamics of canopy-scale photosynthesis. *Ecol. Appl.* **25**, 99–115 (2015).
32. J. Peñuelas, P. Ciais, J. G. Canadell, I. A. Janssens, M. Fernández-Martínez, J. Carnicer, M. Obersteiner, S. Piao, R. Vautard, J. Sardans, Shifting from a fertilization-dominated to a warming-dominated period. *Nat. Ecol. Evol.* **1**, 1438–1445 (2017).
33. N. Forsell, O. Turkovska, M. Gusti, M. Obersteiner, M. den Elzen, P. Havlik, Assessing the INDCs' land use, land use change, and forest emission projections. *Carbon Balance Manag.* **11**, 26 (2016).

34. M. W. van der Kamp, E. J. Prentice, K. L. Kraakman, M. Connolly, A. J. Mulholland, V. L. Arcus, Dynamical origins of heat capacity changes in enzyme-catalysed reactions. *Nat. Commun.* **9**, 1–7 (2018).
35. D. Papale, M. Reichstein, M. Aubinet, E. Canfora, C. Bernhofer, W. Kutsch, B. Longdoz, S. Rambal, R. Valentini, T. Vesala, D. Yakir, Towards a standardized processing of Net Ecosystem Exchange measured with eddy covariance technique: Algorithms and uncertainty estimation. *Biogeosciences* **3**, 571–583 (2006).
36. G. Lasslop, M. Reichstein, D. Papale, A. D. Richardson, A. Arneth, A. Barr, P. Stoy, G. Wohlfahrt, Separation of net ecosystem exchange into assimilation and respiration using a light response curve approach: Critical issues and global evaluation. *Glob. Chang. Biol.* **16**, 187–208 (2010).
37. C. R. Schwalm, C. A. Williams, K. Schaefer, A. Arneth, D. Bonal, N. Buchmann, J. Chen, B. E. Law, A. Lindroth, S. Luyssaert, Assimilation exceeds respiration sensitivity to drought: A FLUXNET synthesis. *Glob. Change Biol.* **16**, 657–670 (2010).
38. M. Jung, S. Koirala, U. Weber, K. Ichii, F. Gans, G. Camps-Valls, D. Papale, C. Schwalm, G. Tramontana, M. Reichstein, The FLUXCOM ensemble of global land-atmosphere energy fluxes. *Sci. Data.* **6**, 1–14 (2019).
39. C. J. Still, J. A. Berry, G. J. Collatz, R. S. DeFries, Global distribution of C_3 and C_4 vegetation: Carbon cycle implications. *Glob. Biogeochem. Cycles.* **17**, 1006–1014 (2003).
40. G. J. Collatz, J. A. Berry, J. S. Clark, Effects of climate and atmospheric CO_2 partial pressure on the global distribution of C_4 grasses: Present, past, and future. *Oecologia* **114**, 441–454 (1998).

Acknowledgments: We wish to acknowledge D. Huntzinger for support of this concept; C. Truettneter for WorldClim data support; K. Schmidt, M. Hurteau, and P. Fulé for feedback on framing; and D. Sonderegger for feedback on uncertainty analysis. This work used eddy covariance data acquired and shared by the FLUXNET community, including these networks: AmeriFlux, AfriFlux, AsiaFlux, CarboAfrica, CarboEuropeIP, CarboItaly, CarboMont, ChinaFlux, Fluxnet-Canada, GreenGrass, ICOS, KoFlux, LBA, NECC, OzFlux-TERN, TCOS-Siberia, and USCCC. The ERA-Interim reanalysis data are provided by ECMWF and processed by LSCE. The FLUXNET eddy covariance data processing and harmonization were carried out by the European Fluxes Database Cluster, AmeriFlux Management Project, and Fluxdata project of FLUXNET, with the support of CDIAC and ICOS Ecosystem Thematic Center, and the OzFlux, ChinaFlux, and AsiaFlux offices. **Funding:** Funding for this research was provided by the National Aeronautics and Space Administration (NASA) (grant NNX12AK12G), National Science Foundation (NSF) East-Asia Pacific Summer Institute Fellowship (1614404), Royal Society of New Zealand Foreign Partnership Programme (EAP-UOW1601), and New Zealand Marsden Fund (grant 16-UOW-027). **Author contributions:** K.A.D., C.R.S., V.L.A., and L.A.S. designed the analysis. K.A.D. carried out the analysis with support from L.L.L. K.A.D. wrote the manuscript with contributions from all authors. C.R.S. and G.W.K. contributed significantly to the framing of the paper. **Competing interests:** The authors declare that they have no competing interests. **Data and materials availability:** FLUXNET data access depends on the tier of data used. Tier 1 data are open and free for scientific and educational purposes, and their use follows the fair use policy accessed at https://fluxnet.fluxdata.org/data/data-policy/. Tier 2 data are from producers who are currently unable to share their data in an open manner and require an approved proposal for data access. Data access proposal information can be found at https://fluxnet.fluxdata.org/. A list of FLUXNET sites from tiers 1 and 2 can be found in the Supplementary Materials (table S3). Downscaled WorldClim CMIP5 climate data are freely available at http://worldclim.org/CMIP5v1. Upscaled FLUXNET data used to evaluate biosphere productivity are freely available at www.fluxcom.org/. An open repository with code used to fit MMRT along with parameters derived for each FLUXNET site used in this analysis are available at https://github.com/katharynduffy/TmaxLandUptake. Gridded T_P^{max} generated from this analysis along with CMIP5 multimodel means, and gridded biosphere productivity, which is affected by T_P^{max} are freely available at https://doi.pangaea.de/10.1594/PANGAEA.893266.

Submitted 20 May 2019
Accepted 20 November 2020
Published 13 January 2021
10.1126/sciadv.aay1052

Citation: K. A. Duffy, C. R. Schwalm, V. L. Arcus, G. W. Koch, L. L. Liang, L. A. Schipper, How close are we to the temperature tipping point of the terrestrial biosphere? *Sci. Adv.* **7**, eaay1052 (2021).